INTERNATIONAL JOURNAL FOR NUMERICAL METHODS IN FLUIDS
Int. J. Numer. Meth. Fluids **29**: 749–763 (1999)

NAVIER–STOKES SOLUTIONS OF LAMINAR FLOWS BASED ON ORTHOGONAL HELICAL CO-ORDINATES

T.J. HÜTTL*, C. WAGNER AND R. FRIEDRICH

Lehrstuhl für Fluidmechanik, Technische Universität München, Boltzmannstr. 15, D-85747 Garching, Germany

SUMMARY

In this paper a numerical method to compute time-dependent flows in helically coiled pipes with circular cross-section and constant curvature κ and torsion τ is presented. The incompressible Navier–Stokes equations, explicitly derived in an orthogonal helical co-ordinate system, are integrated numerically. The results show for example, the influence of curvature and torsion on the axial velocity profile. Good agreement with experiment is found. The numerical simulations also allow a detailed study of the secondary motion in the cross-section of the pipe by considering vector plots and contour lines of the streamfunction. Furthermore, the formation of a pressure distribution perpendicular to the pipe axis is shown. Besides the Reynolds number, other characteristic flow parameters, like the Dean numer *De*, and the Germano number *Gn*, are used to compare the flow through different pipe configurations. Copyright © 1999 John Wiley & Sons, Ltd.

KEY WORDS: laminar; pipe flow; curvature; torsion; helical pipe; secondary flow

1. INTRODUCTION

Fluid flow through curved or helically coiled pipes is very common. It can be found in nature, e.g. in blood vessels, particularly the aorta, the trachea or in water ducts for plants. Curved pipes, bends and coils are also of great importance in industrial applications in many branches of engineering. Heat exchangers, chemical reactors, exhaust gas ducts of engines, cooling channels in the nozzle of a rocket engine or any kind of pipelines, tubes and conduits transporting gases and liquids profit from the use of curved or helically coiled pipes due to the possibility of satisfying space and/or geometric requirements, and due to the characteristics of the induced secondary flow, which influences the heat and mass transfer.

The subject of the present investigation is the steady state, fully developed laminar flow of an incompressible, Newtonian fluid in several pipes with circular cross-section, constant curvature κ and torsion τ. Although the theoretical and experimental investigation of flow in pipes with curvature and torsion in a systematical way is of recent origin, this flow configuration has always been classified as even more complex than the flow through straight ducts. Williams *et al.* [1] notice that the position of maximum axial velocity is moved towards the outer wall of a curved pipe because of centrifugal forces. Later, Eustice [2,3] demonstrated the existence of a secondary flow by injecting ink into water, flowing through a coiled pipe.

* Correspondence to: Lehrstuhl für Fluidmechanik, Technische Universität München, Boltzmannstr. 15, D-85747 Garching, Germany.

CCC 0271–2091/99/070749–15$17.50

Received December 1997
Revised March 1998

Due to the lack of supercomputers some decades ago, the investigators were unable to solve the Navier–Stokes equations numerically. Besides experiments, only analytical solutions of simplified equations were used to investigate the flow in curved and coiled pipes. Dean [4,5] derived a solution of the flow in loosely coiled ($\kappa \ll 1$) pipes and showed the typical secondary flow pattern with two recirculation zones. Besides the Reynolds number Re, a new parameter, which characterizes the magnitude and shape of the secondary motion through a torus, was found. Later, this parameter was defined as the Dean number $De = \kappa^{1/2} Re$. For three differently curved pipes, Adler [6] presented experimental results of laminar and turbulent flow. Since then, a few investigations were reported of toroidal flows without considering torsion effects, e.g. [14]. A good survey of the voluminous research activities in this area and related topics is given by Berger *et al.* [7] and additional aspects can be found in Ito [8].

Wang [9] solved helical flow problems with small curvature and small torsion using a perturbation method based on a non-orthogonal helical co-ordinate system. By extending the Dean equations to a helical pipe flow, Germano [10,11] studied the same problem by introducing an orthogonal co-ordinate system. In order to describe the torsion effect on the flow, a third dimensionless parameter has been defined: the torsion number or the Germano number $Tn = Gn = \tau Re$. In an extensive study of helical pipe flow by using a separation method, Liu and Masliyah [12] showed that another dimensionless group of parameters emerges. The critical values $\lambda > 0.2$ and $\lambda^* > 0.039$ of the Liu–Masliyah parameters $\lambda = GnDe^{-3/2}$ for $De \geq 20$ and $\lambda^* = GnDe^{-2}$ for $De < 20$ mark the change of the secondary flow pattern from two vortices to one vortex.

In this study a finite volume method on a three-dimensional staggered grid with a semi-implicit time integration scheme is used to study the laminar flow in straight, curved and helically coiled pipes for different pipe geometries and flow conditions. This study concentrates on steady, fully developed helical pipe flow with periodic in- and outflow boundary conditions. Since this flow is axially invariant, it changes only in the circular cross-section of the pipe. Contour lines and profiles of the axial velocity will be presented. The profiles are compared with experimental results. The induced secondary flow is demonstrated by means of vector plots and contour lines of the streamfunction. Furthermore, the formation of a pressure distribution perpendicular to the pipe axis is also shown by contour lines.

2. GEOMETRY AND GOVERNING EQUATIONS

The geometry of a helical pipe can be viewed as a pipe of radius R, wound around a cylinder of constant radius $(r_a - R)$ (see Figure 1). With the pitch p_s, defined by the increase in elevation per revolution of coils $2\pi p_s$, the curvature κ and the torsion τ of the helical pipe axis can be calculated from

$$\kappa = \frac{r_a}{(r_a^2 + p_s^2)} \tag{1}$$

and

$$\tau = \frac{p_s}{(r_a^2 + p_s^2)}. \tag{2}$$

As introduced by Germano [10,11], a helical co-ordinate system can be established in reference to the master Cartesian co-ordinate system. By using the helical co-ordinates s for axial direction, r for radial direction and θ for circumferential direction, the position of any given point X inside the helical pipe can be described by the vector $\vec{x}$ as:

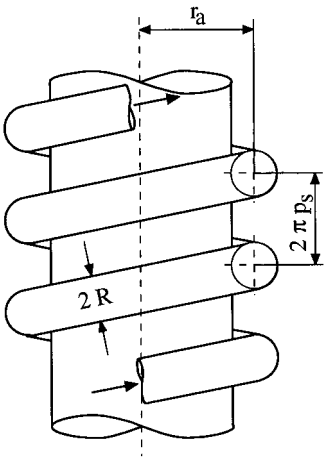

Figure 1. Helically coiled pipe.

$$\vec{x} = \vec{P}(s) - r\,\sin(\theta - \tau s)\vec{N}(s) + r\,\cos(\theta - \tau s)\vec{B}(s). \tag{3}$$

Here $\vec{T}$, $\vec{N}$ and $\vec{B}$ are the tangential, normal and binormal directions to the generic curve of the pipe axis at the point of consideration (see Figure 2). The metric of the orthogonal helical co-ordinate system is given by

$$\mathrm{d}\vec{x}\cdot\mathrm{d}\vec{x} = (1 + \kappa r\,\sin(\theta - \tau s))^2\,\mathrm{d}s^2 + \mathrm{d}r^2 + r^2\,\mathrm{d}\theta^2, \tag{4}$$

where $\mathrm{d}s$, $\mathrm{d}r$ and $\mathrm{d}\theta$ are the infinitesimal increments in the axial, radial and circumferential directions. With this metric, one obtains the scale factors h_s, h_r and h_θ, that are used to express the Navier–Stokes equations in helical co-ordinates:

$$h_s = 1 + \kappa r\,\sin(\theta - \tau s), \tag{5}$$

$$h_r = 1, \tag{6}$$

$$h_\theta = r. \tag{7}$$

The Navier–Stokes equations read in an orthogonal helical co-ordinate system [13]:

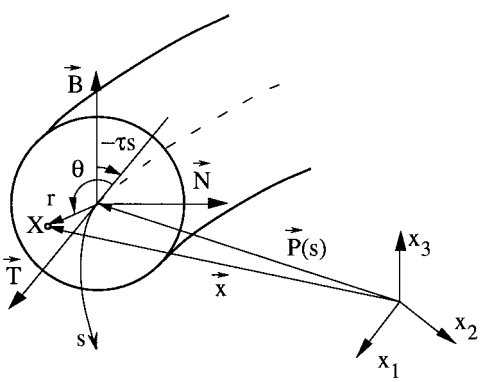

Figure 2. Description of the orthogonal helical (s, r, θ) coordinate system, as introduced by Germano [10,11].

Continuity equation:

$$\frac{\partial}{\partial s}(ru_s)+\frac{\partial}{\partial r}(h_s r u_r)+\frac{\partial}{\partial \theta}(h_s u_\theta)=0. \tag{8}$$

s Momentum:

$$\begin{aligned}
&\frac{\partial u_s}{\partial t}+\frac{1}{h_s}\frac{\partial}{\partial s}(u_s u_s)+\frac{1}{h_s r}\frac{\partial}{\partial r}(h_s r u_s u_r)+\frac{1}{h_s r}\frac{\partial}{\partial \theta}(h_s u_s u_\theta)+\frac{\kappa\,\sin(\theta-\tau s)}{h_s}u_s u_r+\frac{\kappa\,\cos(\theta-\tau s)}{h_s}u_s u_\theta\\
&=-\frac{1}{h_s}\frac{\partial p}{\partial s}+\frac{1}{Re_\tau}\left[\frac{2}{h_s}\frac{\partial}{\partial s}\left(\frac{1}{h_s}\left(\frac{\partial u_s}{\partial s}+\kappa\,\sin(\theta-\tau s)u_r+\kappa\,\cos(\theta-\tau s)u_\theta\right)\right)\right.\\
&\quad+\frac{1}{h_s r}\frac{\partial}{\partial r}\left(h_s h_s r\frac{\partial}{\partial r}\left(\frac{u_s}{h_s}\right)+r\frac{\partial u_r}{\partial s}\right)+\frac{1}{h_s r}\frac{\partial}{\partial \theta}\left(\frac{h_s h_s}{r}\frac{\partial}{\partial \theta}\left(\frac{u_s}{h_s}\right)+\frac{\partial u_\theta}{\partial s}\right)\\
&\quad\left.+\kappa\,\sin(\theta-\tau s)\left(\frac{\partial}{\partial r}\left(\frac{u_s}{h_s}\right)+\frac{1}{h_s h_s}\frac{\partial u_r}{\partial s}\right)+\kappa\,\cos(\theta-\tau s)\left(\frac{1}{r}\frac{\partial}{\partial \theta}\left(\frac{u_s}{h_s}\right)+\frac{1}{h_s h_s}\frac{\partial u_\theta}{\partial s}\right)\right].
\end{aligned} \tag{9}$$

r Momentum:

$$\begin{aligned}
&\frac{\partial u_r}{\partial t}+\frac{1}{h_s}\frac{\partial}{\partial s}(u_s u_r)+\frac{1}{h_s r}\frac{\partial}{\partial r}(h_s r u_r u_r)+\frac{1}{h_s r}\frac{\partial}{\partial \theta}(h_s u_r u_\theta)-\frac{\kappa\,\sin(\theta-\tau s)}{h_s}u_s u_s-\frac{u_\theta u_\theta}{r}\\
&=-\frac{\partial p}{\partial r}+\frac{1}{Re_\tau}\left[\frac{1}{h_s}\frac{\partial}{\partial s}\left(h_s\frac{\partial}{\partial r}\left(\frac{u_s}{h_s}\right)+\frac{1}{h_s}\frac{\partial u_r}{\partial s}\right)+\frac{2}{h_s r}\frac{\partial}{\partial r}\left(h_s r\frac{\partial u_r}{\partial r}\right)+\frac{1}{h_s}\frac{\partial}{\partial \theta}\left(h_s\left(\frac{1}{rr}\frac{\partial u_r}{\partial \theta}+\frac{\partial}{\partial r}\left(\frac{u_\theta}{r}\right)\right)\right)\right.\\
&\quad\left.-\frac{2\kappa\,\sin(\theta-\tau s)}{h_s h_s}\left(\frac{\partial u_s}{\partial s}+\kappa\,\sin(\theta-\tau s)u_r+\kappa\,\cos(\theta-\tau s)u_\theta\right)-\frac{2}{rr}\left(\frac{\partial u_\theta}{\partial \theta}+u_r\right)\right].
\end{aligned} \tag{10}$$

θ Momentum:

$$\begin{aligned}
&\frac{\partial u_\theta}{\partial t}+\frac{1}{h_s}\frac{\partial}{\partial s}(u_s u_\theta)+\frac{1}{h_s r}\frac{\partial}{\partial r}(h_s r u_r u_\theta)+\frac{1}{h_s r}\frac{\partial}{\partial \theta}(h_s u_\theta u_\theta)-\frac{\kappa\,\cos(\theta-\tau s)}{h_s}u_s u_s+\frac{1}{r}u_r u_\theta\\
&=-\frac{1}{r}\frac{\partial p}{\partial \theta}+\frac{1}{Re_\tau}\left[\frac{1}{h_s}\frac{\partial}{\partial s}\left(\frac{h_s}{r}\frac{\partial}{\partial \theta}\left(\frac{u_s}{h_s}\right)+\frac{1}{h_s}\frac{\partial u_\theta}{\partial s}\right)+\frac{1}{h_s r}\frac{\partial}{\partial r}\left(h_s\left(\frac{\partial u_r}{\partial \theta}+rr\frac{\partial}{\partial r}\left(\frac{u_\theta}{r}\right)\right)\right)\right.\\
&\quad+\frac{2}{h_s rr}\frac{\partial}{\partial \theta}\left(h_s\left(\frac{\partial u_\theta}{\partial \theta}+u_r\right)\right)-\frac{2\kappa\,\cos(\theta-\tau s)}{h_s h_s}\left(\frac{\partial u_s}{\partial s}+\kappa\,\sin(\theta-\tau s)u_r+\kappa\,\cos(\theta-\tau s)u_\theta\right)\\
&\quad\left.+\left(\frac{1}{rr}\frac{\partial u_r}{\partial \theta}+\frac{\partial}{\partial r}\left(\frac{u_\theta}{r}\right)\right)\right].
\end{aligned} \tag{11}$$

They are written in dimensionless form. The pipe radius R, the mean friction velocity u_τ and the time $t_{\mathrm{ref}}=R/u_\tau$ are used as scaling variables. The dimensionless mass density is set to 1. The mean friction velocity is defined as the square root of the mean wall shear stress as follows:

$$u_\tau=\sqrt{\frac{\tau_{w,m}}{\rho}}, \tag{12}$$

$$\tau_{w,m}=\frac{1}{2\pi}\int_{\theta=0}^{2\pi}\tau_w(\theta)\,\mathrm{d}\theta. \tag{13}$$

The dimensionless curvature $\kappa = R\kappa'$ and torsion $\tau = R\tau'$ are non-dimensionalized by the pipe radius R.

The Reynolds, Dean and Germano numbers based on these scaling quantities are:

$$Re_\tau = \frac{Ru_\tau}{\nu}, \tag{14}$$

$$De_\tau = \sqrt{\kappa} Re_\tau, \tag{15}$$

$$Gn_\tau = \tau Re_\tau. \tag{16}$$

3. NUMERICAL METHOD AND BOUNDARY CONDITIONS

A finite volume method on staggered grids is used to discretize the spatial derivatives and source terms in the governing equations. It leads to central differences of second-order accuracy for the mass and momentum fluxes across the cell faces. A semi-implicit time-integration scheme treats all those convection and diffusion terms implicitly that contain derivatives in the θ-direction. The remaining convection terms are integrated in time with a second-order-accurate leapfrog step. An averaging step of all the 50 time steps avoids possible $2\Delta t$ oscillations. Diffusive terms with derivatives in the s- and r-directions are treated with a first-order Euler backward step. The size of the time step is selected according to a linear stability argument. The use of a projection step leads to a 3D Poisson problem for the pressure correction, which is solved by a conjugate gradient method for unsymmetric matrices.

Boundary conditions are required for all boundaries of the computational domain. At the walls, impermeability and no-slip boundary conditions are realized. Velocity components that are needed on the pipe axis are obtained by interpolation across the axis. In the circumferential direction, all variables are periodic by definition. In the axial direction, periodic boundary conditions are used. For helically coiled pipes, the rotation of the co-ordinate system along the pipe axis must be taken into account and the perfect matching of the cells at the in- and outflow boundaries must be ensured by choosing a suitable combination of axial length and number of grid points in the θ-direction (see Figure 3).

The flow is driven in the axial direction by means of a pressure gradient $\Delta P/\Delta s$, which must balance the viscous friction along the pipe wall.

4. COMPUTATIONAL DETAILS

The length of the computational domain Δs along the axial co-ordinate s was taken to be $0.5R$ for toroidal pipe flow. For helical pipe flow, it was between $0.1257R$ and $125.7R$ as it has to satisfy the condition

$$\Delta s = n \cdot \frac{2\pi}{n_\theta \tau}, \quad n = 1, 2, 3, \ldots \tag{17}$$

in order to fulfill the cell matching. The grid has $n_r = 50$ points in radial, $n_\theta = 50$ points in circumferential and $n_s = 10$ (5) points in the axial direction for helical (toroidal) pipe flow.

The Reynolds numbers

$$Re_\mathrm{b} = \frac{2u_\mathrm{b}R}{\nu}, \tag{18}$$

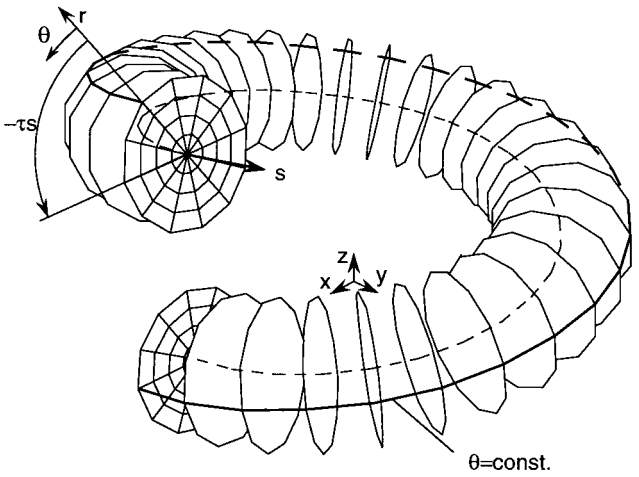

Figure 3. Visualisation of the rotation of the (θ, r) co-ordinate system along the axis.

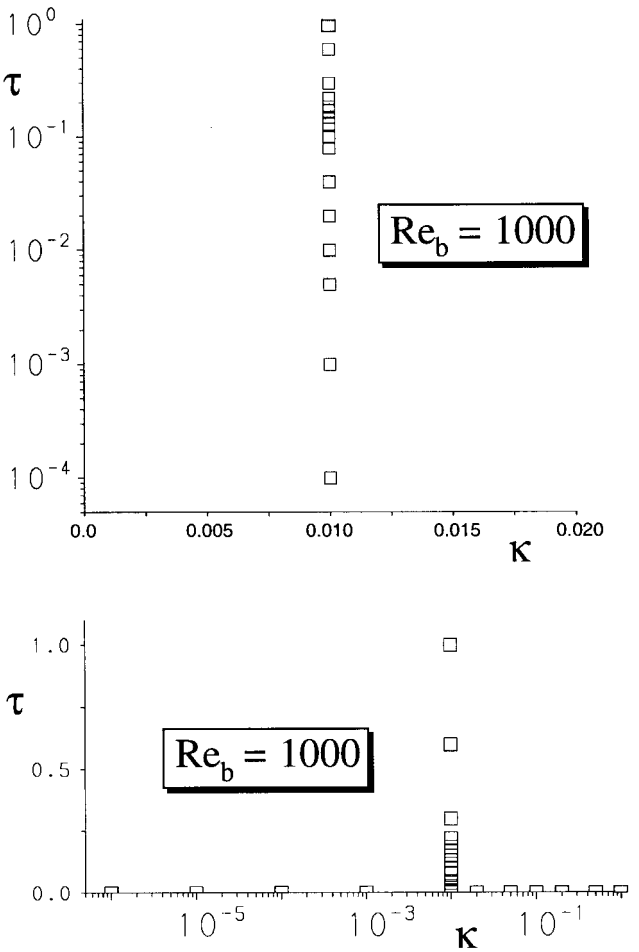

Figure 4. Simulated pipe configurations with $Re_b = 1000$.

based on bulk velocity u_b and pipe diameter $2R$ were varied over the whole laminar flow regime. In this paper, only simulations with $Re_b = 1000$ are presented. The curvature κ ranges from 0 to 0.99 and the torsion τ from 0 to 1.0, see Figure 4.

The Dean number De_b, and Germano number Gn_b built with this Reynolds number are

$$De_b = \sqrt{\kappa} Re_b, \tag{19}$$

$$Gn_b = \tau Re_b. \tag{20}$$

The simulations were started from a velocity profile for laminar flow in a straight pipe and were terminated when the flow field had converged at the iteratively adjusted Reynolds number Re_b. Figure 5 shows the fast convergence of the Reynolds number Re_τ for $Re_b = 1000$, $\kappa = \tau = 0$ to the Reynolds number $Re_\tau = 44.7$ for fully developed laminar flow in a straight pipe given by

$$Re_\tau = \sqrt{2Re_b}. \tag{21}$$

The computations are carried out on a Fujitsu VPP500 at HLRZ Darmstadt and the Cray Y-MP and Cray T94 at LRZ, München.

5. NUMERICAL RESULTS

5.1. Laminar flow in curved pipes

In a straight pipe, the fully developed flow has a parabolic profile for the axial velocity with the maximum at the pipe axis and no radial or circumferential velocity components. The flow in a torus is influenced by a centrifugal force due to curvature. The centrifugal force on a flow particle is proportional to its velocity squared and the curvature of the particle path. Near the wall, where the velocity is small, the centrifugal force is also small. In the core of the torus cross-section, where the velocity is high, the centrifugal force accelerates the flow outwards to the wall. In principle, the centrifugal force is balanced by a pressure gradient in the plane perpendicular to the pipe axis. However, near the wall this pressure gradient can no longer be balanced by the flow and consequently the flow is forced inwards and finally towards the center of the torus. Due to continuity, the rapidly moving central part of the flow is forced outward. The flow in the plane perpendicular to the mean flow is called the secondary flow. If the curvature is significant, the axial velocity profile will be completely altered by this secondary motion and a considerable increase in drag is observed. Figure 6(a) shows contour lines of the axial velocity that are symmetric to the horizontal axis. The position of the maximum is forced outwards and the contour lines, which would be circles for flow in a straight pipe, are deformed. Contour lines of the pressure (Figure 6(b)) are almost rectilinear and perpendicular to the horizontal axis in the core of the cross-section. The secondary flow can also be visualized by vector plots (Figure 6(c)) or contour lines of the streamfunction (Figure 6(d)). It can easily be seen that the flow moves outwards in the core region and inwards at the wall. The bifurcation at the outer wall and the confluence at the inner wall divide the upper and lower half of the cross-section into two symmetric recirculation cells, called the Dean cells. The magnitude and shape of the secondary motion, and therefore the shape of the axial velocity, depend on the Dean number De of the flow. Figure 7 shows the influence of the Dean number on the axial velocity profile along the horizontal axis (top) and the vertical axis (bottom) of the cross-section. With increasing De, the position of the maximum axial velocity is forced to the outer wall and its value decreases. The vertical cut

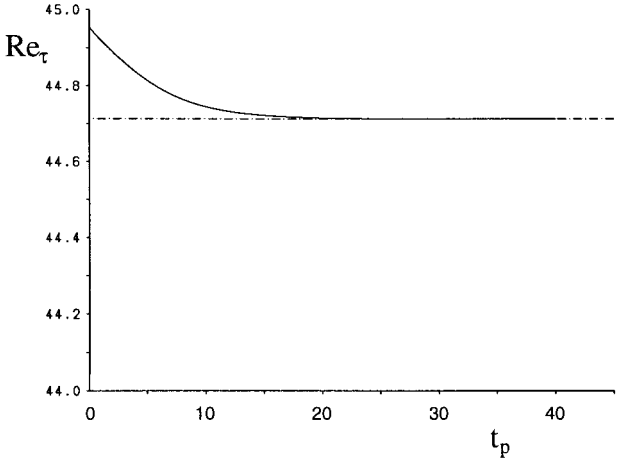

Figure 5. Convergence of the iteratively adjusted Reynolds number $Re_b = 1000$, $\kappa = 0$, $\tau = 0$.

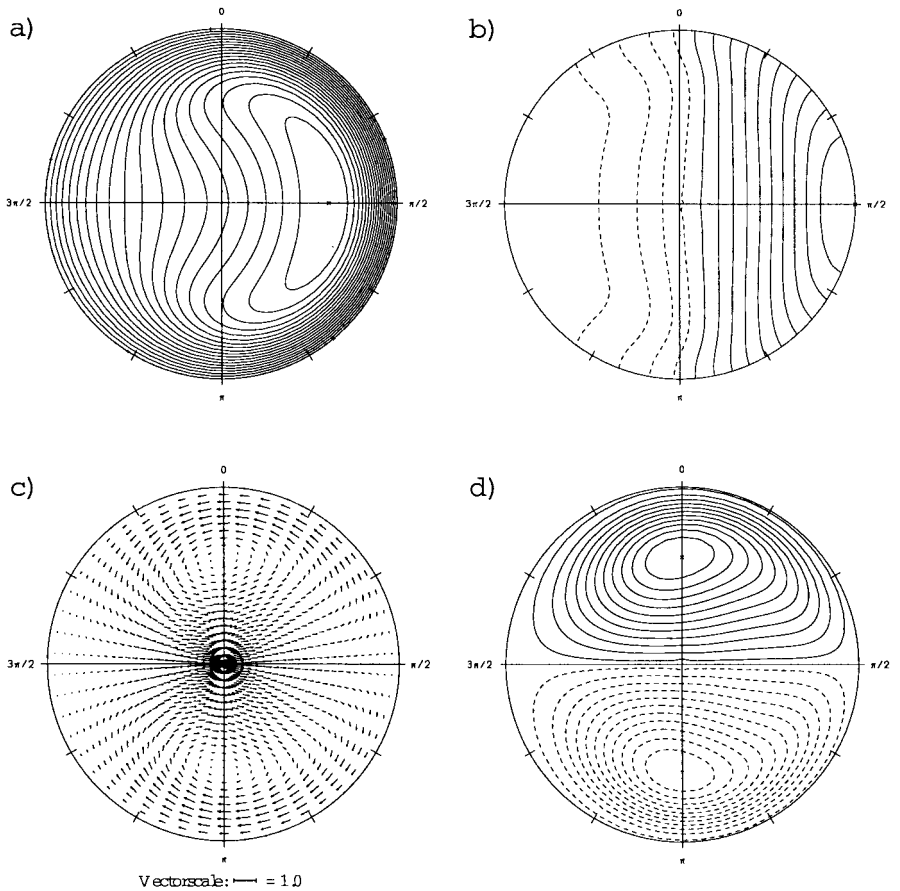

Figure 6. Laminar flow in a curved pipe, $Re_b = 1000$, $\kappa = 0.01$; (a) axial velocity $u_{s,\max} = 15.9$, (b) pressure $p_{\min} = -0.75$, $p_{\max} = 1.65$, (c) vector plot of the secondary flow, (d) contour lines of the streamfunction.

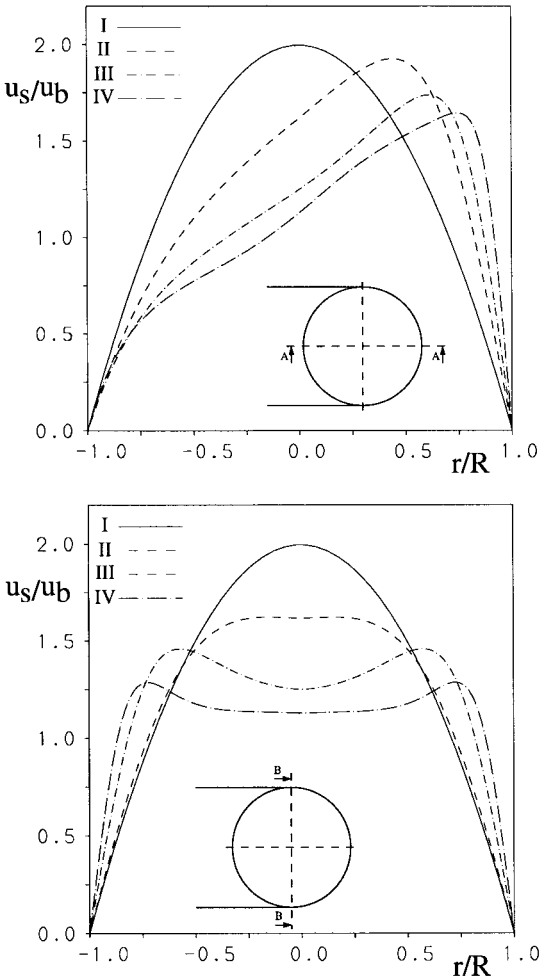

Figure 7. Profiles of the axial velocity for $Re_b = 1000$: (I) $\kappa = 0$, $De_b = 0$, (II) $\kappa = 0.001$, $De_b = 31.62$, (III) $\kappa = 0.01$, $De_b = 100$, (IV) $\kappa = 0.1$, $De_b = 316.22$; top, horizontal cut (A–A); bottom, vertical cut (B–B).

shows the change of the parabolic profile to a more flat profile with two local maxima near the wall. The increase in the radial gradient of the axial velocity leads to an increase of drag in curved pipes.

The axial velocity profiles can be used to compare the numerical results with the experiments performed by Adler [6]. Both cases $Re_b = 1930$, $\kappa = 0.02$ and $Re_b = 3220$, $\kappa = 0.005$ show good agreement between simulation and experiment (see Figure 8).

5.2. Laminar flow in helically coiled pipes

The flow in curved pipes is influenced by the centrifugal force, a kind of inertia force. The inertia forces have a more complicated effect on the flow when the bounding geometry of the pipe wall is more complex. In helically coiled pipes, the plane of curvature moves and rotates and therefore, the direction of the inertia force changes along the axis. For loosely coiled pipes with small curvature $\kappa \leq 0.01$ and small torsion $\tau \leq 0.01$, the effect of curvature is dominant and the torsion effect is negligible.

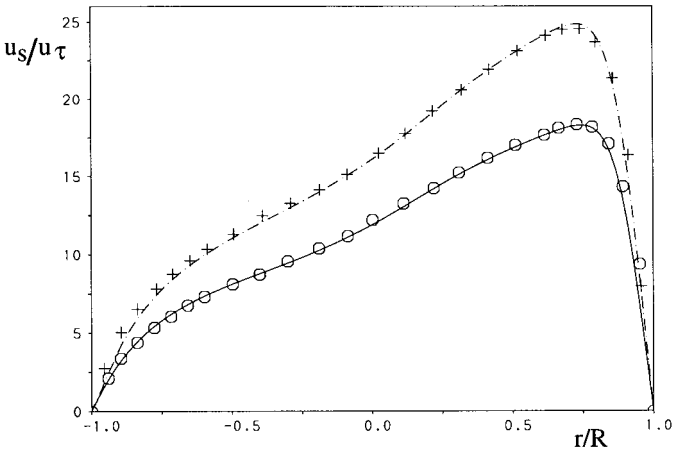

Figure 8. Comparison of axial velocity profiles of the numerical simulations (lines) with experiments by Adler [6] (symbols). Upper profile, $Re_b = 3220$, $\kappa = 0.005$, $De_b = 227.7$; lower profile, $Re_b = 1930$, $\kappa = 0.02$, $De_b = 272.9$.

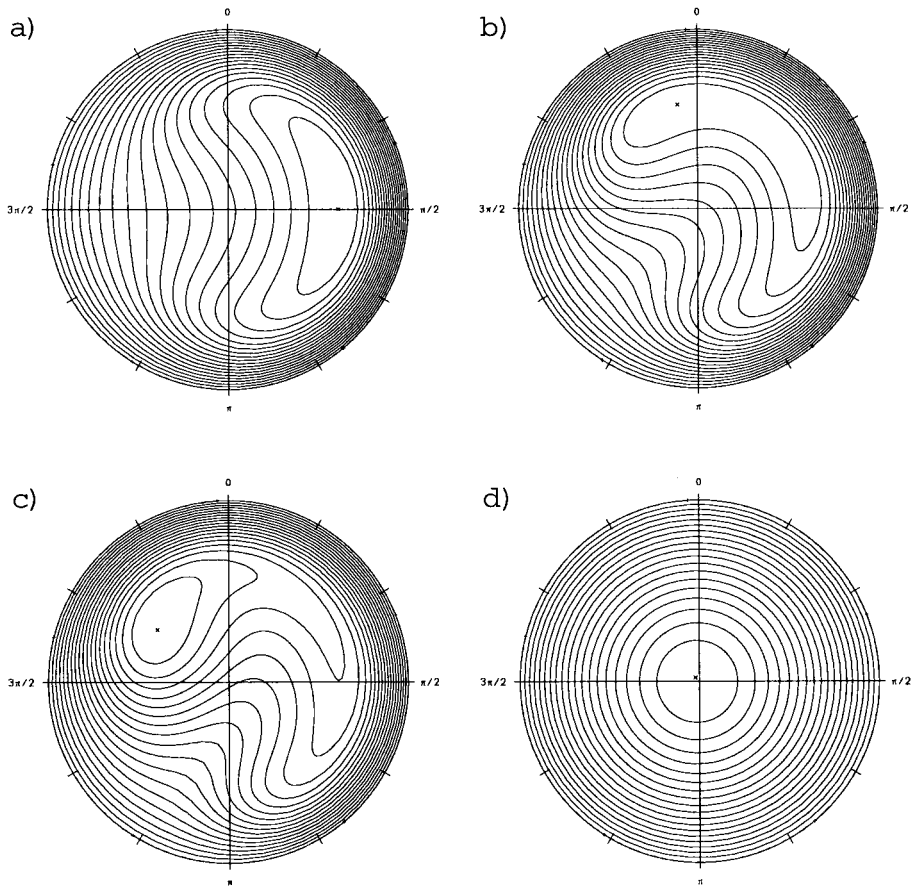

Figure 9. Contour lines of axial velocity of flow through helically coiled pipes: $Re_b = 1000$, $\kappa = 0.01$; (a) $\tau = 0.01$; (b) $\tau = 0.0995$; (c) $\tau = 0.13$; (d) $\tau = 1.0$.

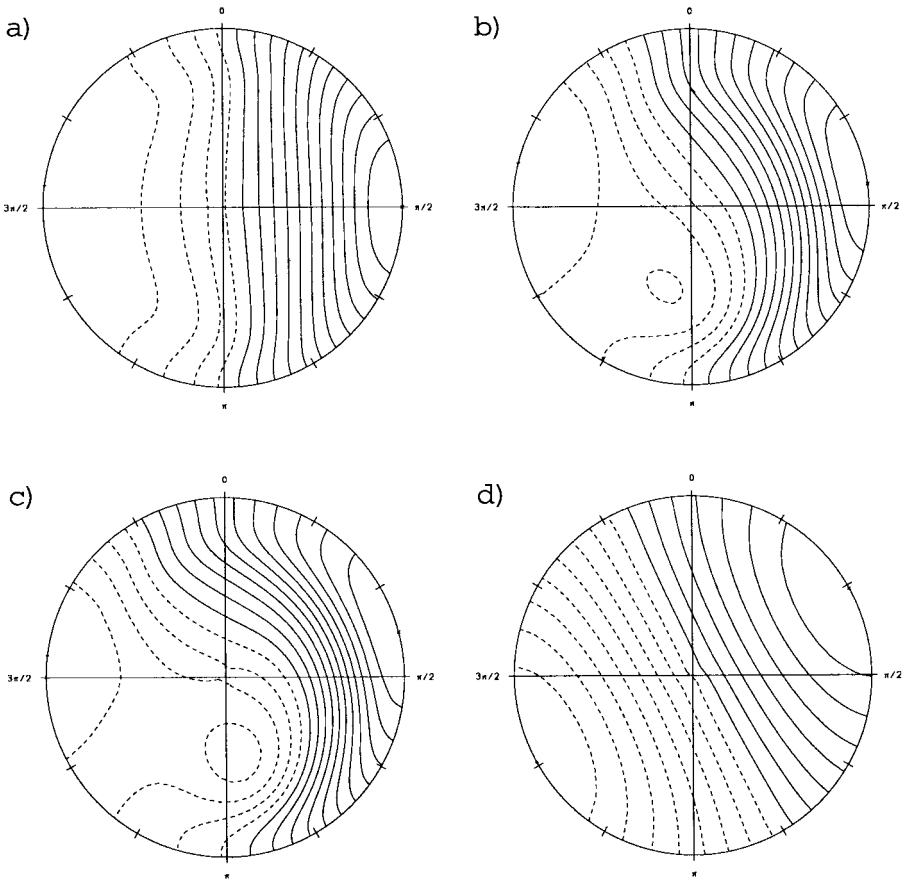

Figure 10. Contour lines of the pressure distribution in a cross section of helically coiled pipes: $Re_b = 1000$, $\kappa = 0.01$; (a) $\tau = 0.01$; (b) $\tau = 0.0995$; (c) $\tau = 0.13$; (d) $\tau = 1.0$.

With the increase of torsion, the torsion effect becomes visible. Figure 9 shows contour lines of axial velocity profiles for fixed Reynolds number $Re_b = 1000$ and fixed curvature $\kappa = 0.01$. For small values of torsion, the symmetric pattern is just slightly rotated counter-clockwise. With increasing torsion, the counter-clockwise rotation gets bigger, the pattern is slightly deformed and the symmetry is destroyed. Additionally, increasing the torsion, results in strongly distorted contours of the axial velocity with a maximum moving in counter-clockwise direction. Finally, the position of the maximum of the axial velocity moves back to the axis leading to contour lines that are similar to those of straight pipe flow.

It is known from curved pipe flow that in a cross-section, perpendicular to the pipe axis, a pressure distribution is built up, which is symmetric with respect to the plane in which the axis lies. For increasing torsion, the formerly nearly rectilinear contour lines of the pressure become curved and more complex (see Figure 10). The formation of a local pressure minimum can be observed for higher Germano numbers. This pressure minimum rotates counter-clockwise with increasing torsion and finally disappears again (Figure 10(d)).

An even stronger effect has the torsion on the secondary flow. Figure 11(a) shows that the secondary flow consists of two vortices. An increase in torsion results in the lower vortex gaining in size. The upper vortex becomes very small and weak and Liu and Masliyah [12] observed that the upper cell can disappear. For further increases in torsion, the upper vortex starts to gain in size and strength and the positions of the two vortices are left and right. In the core of the cross-section, the secondary flow is very strong and its direction is upward, while its direction at the inner and outer walls is downward.

The variation of the axial wall shear stress distribution along the pipe wall circumference is shown by polar diagrams in Figure 12. Here, the value of the axial wall shear stress is the polar distance from the origin of each plot. In a straight pipe, the wall shear stress is uniformly distributed. For curved pipe flow, the axial wall shear stress is higher near the outer wall and lower near the inner wall. For helically coiled pipes, the maximum axial wall shear stress moves towards the inner upper wall.

The good agreement between the present simulation and the simulation performed by Liu and Masliyah [12] is presented in Figure 13. These authors predicted the same location of the

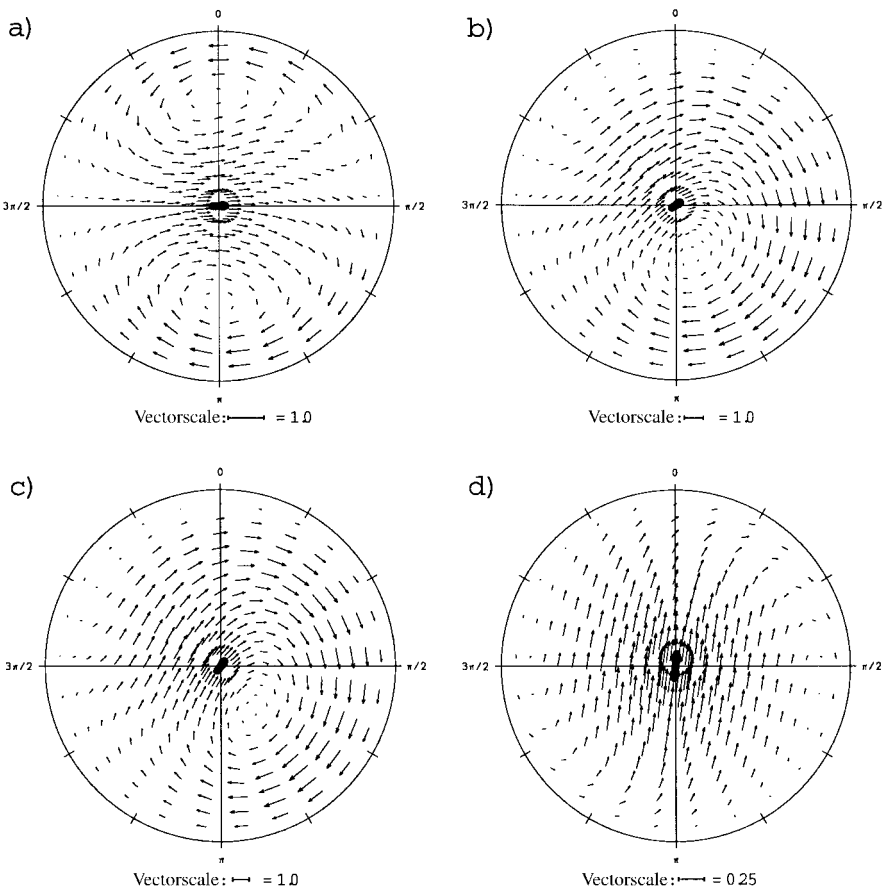

Figure 11. Vector plots of the secondary flow through helically coiled pipes: $Re_b = 1000$, $\kappa = 0.01$; (a) $\tau = 0.01$ b) $\tau = 0.0995$ c) $\tau = 0.13$ d) $\tau = 1.0$.

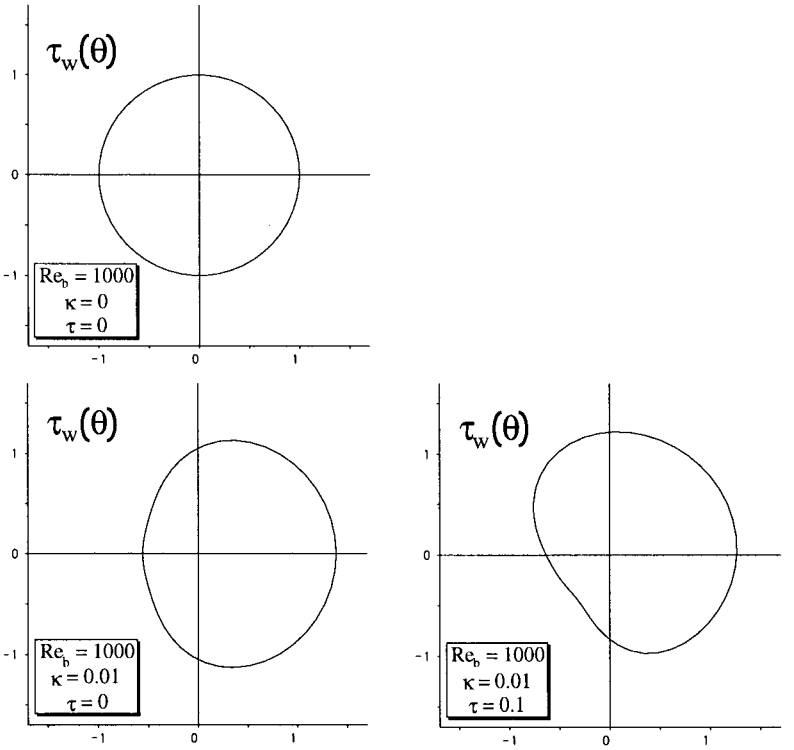

Figure 12. Polar diagram of the axial wall shear stress distribution across the pipe wall circumference for straight, curved and helically coiled pipe.

maximum of the axial velocity and the position of the secondary flow cells. In a perspective plot of the pressure the local minimum can be seen very clearly.

6. CONCLUSIONS

In order to predict the flow in helically coiled pipes, a finite volume code was developed that integrates the incompressible Navier–Stokes equations in an orthogonal helical co-ordinate system. Several flow configurations, namely curved pipes and helically coiled pipes, were simulated and compared. The movement of the position of maximal axial velocity to the outer wall with increasing curvature and the distortion of the contour lines with increasing torsion was shown in detail. The origin of secondary flow with two recirculation cells due to curvature effects and the change of the secondary flow pattern due to torsion effects has been visualized. A comparison with experiments by Adler [6] showed good agreement.

As a next step, direct numerical simulation of fully developed turbulent flow in coiled pipes is envisaged with the aim of studying turbulent transport, production, dissipation and redistribution mechanisms.

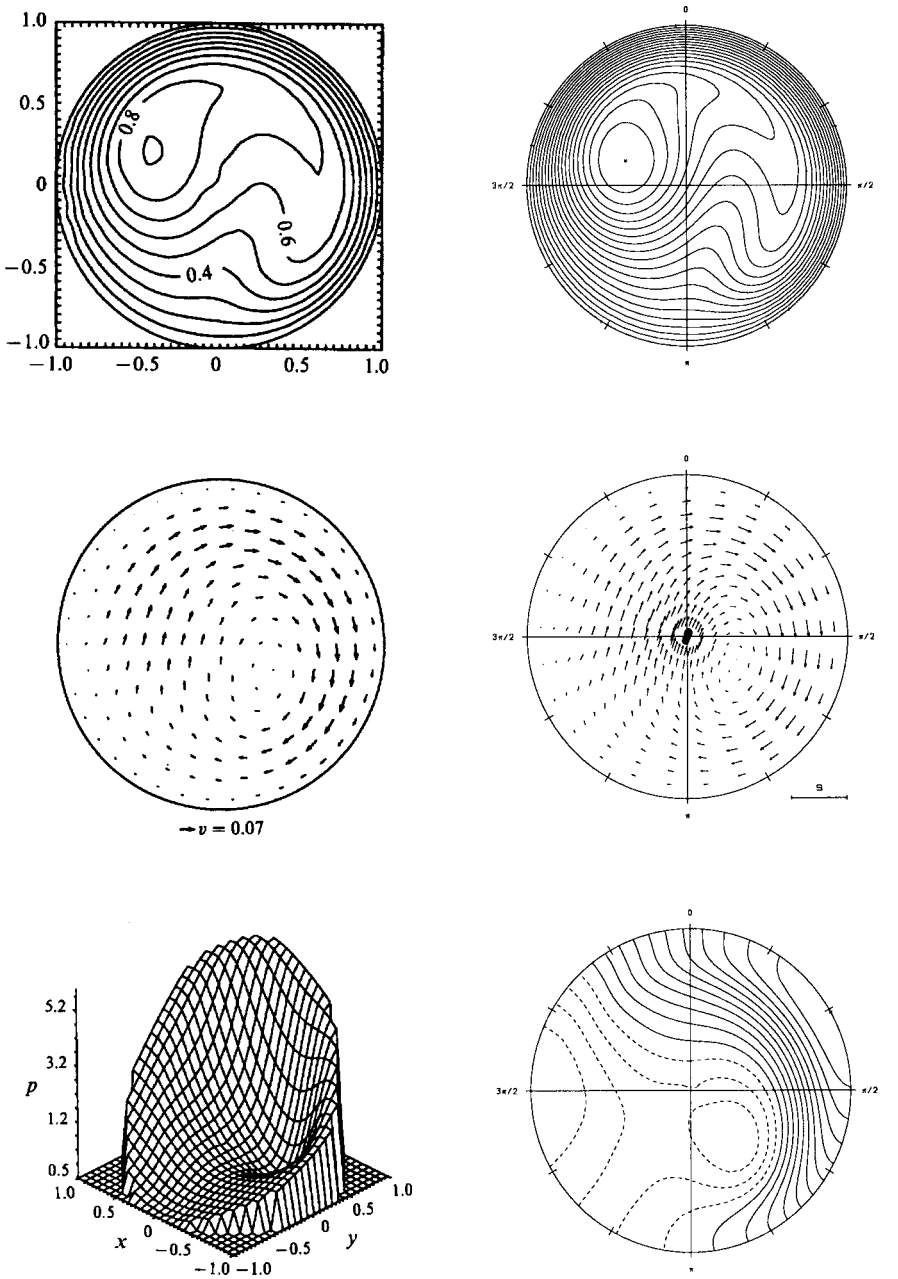

Figure 13. Comparison of the present simulations (right) with the simulations performed by Liu and Masliyah [12] for $Re_b = 1000$, $De_b = 100$, $Gn_b = 150$. First line: axial velocity component; second line: secondary flow vectors; third line: pressure distribution in a cross-section.

ACKNOWLEDGMENTS

The authors are grateful to Professor Germano for stimulating work in this field and for valuable comments.

REFERENCES

1. G.S. Williams, C.W. Hubbell and G.H. Fenkell, 'Experiments at Detroit, MI, on the effect of curvature upon the flow of water in pipes', *Trans. ASCE*, **47**, 1–196 (1902).
2. J. Eustice, 'Flow of water in curved pipes', *Proc. R. Soc. Lond. Ser. A*, **84**, 107–118 (1910).
3. J. Eustice, 'Experiments on streamline motion in curved pipes', *Proc. R. Soc. Lond. Ser. A*, **85**, 119–131 (1911).
4. W.R. Dean, 'Note on the motion of fluid in a curved pipe', *Philos. Mag.*, **4**, 208–223 (1927).
5. W.R. Dean, 'The streamline motion of fluid in a curved pipe', *Philos. Mag.*, **5**, 673–695 (1928).
6. M. Adler, 'Strömung in gekrümmten Rohren', *Z. Angew. Math. Mech.*, **14**, 257–275 (1934).
7. S.A. Berger, L. Talbot and L.-S. Yao, 'Flow in curved pipes', *Annu. Rev. Fluid Mech.*, **15**, 461–512 (1983).
8. H. Ito, 'Flow in curved pipes', *JSME Int. J.*, **30**, 543–552 (1987).
9. C.Y. Wang, 'On the low Reynolds number flow in a helical pipe', *J. Fluid Mech.*, **108**, 185–194 (1981).
10. M. Germano, 'On the effect of torsion on a helical pipe flow', *J. Fluid Mech.*, **125**, 1–8 (1982).
11. M. Germano, 'The Dean equations extended to a helical pipe flow', *J. Fluid Mech.*, **203**, 289–305 (1989).
12. S. Liu and J.H. Masliyah, 'Axially invariant laminar flow in helical pipes with a finite pitch', *J. Fluid Mech.*, **251**, 315–353 (1993).
13. T.J. Hüttl, 'Simulationsprogramm HELIX: Ein FiniteVolumen Verfahren zur Lösung der inkompressiblen 3D Navier–Stokes Gleichungen für Rohrgeometrien mit Krümmung und Torsion, Lehrstuhl für Fluidmechanik', TU München, Bericht *TUM-FLM-96/29*, 1996.
14. B.J. Boersma and F.T.M. Nieuwstadt, 'Large-eddy simulation of turbulent flow in a curved pipe', *10th Symp. on Turbulent Shear Flows*, *Poster Session*, The Pennsylvania State University, 1995, pp. P1-19–P1-24.

